Hybrid Rocket Fuel Regression Rate Data and Modeling

Article · July 2006

DOI: 10.2514/6.2006-4504

2 authors:

Gregory G. Zilliac
NASA
79 PUBLICATIONS **1,882** CITATIONS
SEE PROFILE

Arif Karabeyoglu
Koc University
71 PUBLICATIONS **1,434** CITATIONS
SEE PROFILE

42nd AIAA/ASME/SAE/ASEE Joint Propulsion Conference & Exhibit
9-12 July 2006, Sacramento, California

AIAA 2006-4504

Hybrid Rocket Fuel Regression Rate Data and Modeling

Greg Zilliac*
NASA Ames Research Center, Moffet Field, Mountain View, CA 94035

And

M. Arif Karabeyoglu†
Stanford University, Stanford, CA 94305

Abstract

Hybrid rocket fuel average regression rate is one of the most important values to accurately determine in the hybrid rocket design process and for rocket performance prediction. Yet there is no comprehensive theory that can be used to reliably predict this quantity. Additionally, regression rate data is difficult to measure. Measured data often contains a high degree of scatter, suffers from scale effects and is generally a closely held secret by those performing the experiments and therefore is unavailable for many propellant combinations. This paper presents a regression rate model that has been developed based on the results of several previous studies. The model is applicable to vaporizing fuels in a cylindrical grain configuration that do not form significant char or melt layers. It accounts for the presence of a pre-combustion chamber upstream of the fuel grain and also for variable gas properties (to a limited degree). The model is compared with existing published regression rate data. The results of the comparison are reasonable given the level of approximation in the model but additional work is required before models of this type will supplant regression rate measurements for rocket design purposes.

Nomenclature

a	= Regression rate coefficient	L	= Grain length or characteristic length
A	= Grouping of variables	l	= Temperature ratio exponent
c_p	= Specific heat at constant pressure	M	= Molecular weight
D	= Port diameter	m	= Length exponent for a slab grain
E_a	= Activation energy	$\dot{m}$	= Mass flow rate
G	= Local instantaneous mass flux	$\dot{m}_{ox}$	= Oxidizer mass flow rate
G_{ox}	= Oxidizer mass flux	n	= Flux exponent or f exponent
H	= Channel height	O/F	= Oxidizer to fuel ratio
h	= Enthalpy or heat transfer coefficient	$\dot{Q}$	= Rate of heat transfer
h_v	= Effective heat of gasification	$\bar{\#}$	= Spatially-averaged quantity
k	= Conductivity or Re_D exponent	$\hat{\#}$	= Temporally-averaged quantity

* Research Scientist, NASA Ames Research Center/M.S. 260-1, Member AIAA.
† Research Associate, Dept. of Aeronautics and Astronautics, Stanford University, Member AIAA.

$\hat{\#}$ = Averaged spatially and temporally

R_u = Universal gas constant

r = Radial coordinate (see fig. 1)

$\dot{r}$ = Instantaneous local fuel regression rate

T = Temperature

t_b = Time (burn duration)

u, v = Axial and normal velocity, respectively

x, y = Coordinate system (see fig. 1)

a = Thermal diffusivity

b = Blowing coefficient

d = Boundary layer thickness

e = Emissivity

h = Boundary layer coordinate

q = Boundary layer momentum thickness

m = Absolute viscosity

s = Stefan-Boltzmann constant

r_f = Fuel density

Subscripts

b = Bulk property

bl = Boundary layer

c = Pertaining to the flame

e = Edge of the velocity layer

f = Final or fuel

i = Initial

m = Mean

o = Reference or without blowing

ox = Oxidizer

s = Surface

I. Introduction

In a hybrid rocket engine, the fuel regression rate is the rate that the fuel surface recedes over the course of a burn and this quantity has a first order impact on the configuration (i.e. combustion chamber length and diameter) and therefore the performance of a motor. For example, since the specific impulse of many hydrocarbon fuels burned with a given oxidizer are of similar level, a high regression fuel will result in a combustion chamber design that is shorter and of greater diameter in comparison with a motor that employs a low regression rate fuel (for a single port motor). In order to compare propellants, size a fuel grain, predict the performance of a hybrid motor, and avoid burn-throughs, accurate regression rate data is of paramount importance.

A majority of the existing theories used to analyze hybrid rocket fuel combustion employ a fuel regression rate law that relates the local instantaneous fuel burning rate to the local instantaneous mass flux through the fuel port in terms of an empirically-based power law. This has been the case since Marxman derived such an expression in the first comprehensive theoretical treatment of hybrid rocket fuel combustion[1] in 1963.

Marxman et al.[1, 2] showed that the local instantaneous regression rate $\dot{r}$ of a fuel slab submersed in an oxidizer stream is related to the local instantaneous mass flux G by:

$$\dot{r} = \frac{0.036G}{r_f}\left(\frac{Gx}{m}\right)^{-0.2}\left(\frac{u_e}{u_c}\frac{\Delta h}{h_v}\right)^{0.23} \tag{1}$$

Where $\dot{r}$ is the instantaneous local fuel regression rate, G is the instantaneous local mass flux, x is the distance along the port, u_e/u_c is the velocity ratio of the gas in the main stream to that at the flame, $\Delta h/h_v$ is the ratio of the total enthalpy difference between the flame and fuel surface to the effective heat of vaporization of the fuel and m is the viscosity main stream gas flow (note that the 0.036 coefficient is for English units as originally derived). For a given propellant system, it is typically assumed that $\dot{r}$, G and x are variable and the remaining quantities in equation 1 are constants.

The significance of Marxman's theory is that it identifies many of the factors that influence fuel regression rate and how they are related. Marxman modeled the steady state flow in the port of a hybrid rocket motor as a diffusion flame within a turbulent boundary layer that forms over the regressing fuel surface. Included in his analyses are the effects of conductive and convective heat transfer to the fuel surface and the heat transfer limiting "blocking effect" that results from mass departing the fuel surface into the boundary layer. A radiative heat transfer term (not shown in eq. 1) was also included in an ad hoc fashion but this term is thought to be small for fuels that do not contain metals.

Over the years, the results of many regression rate tests have proven that the functional form of Marxman's regression rate law is valid. Unfortunately, the law as originally derived is not accurate enough for rocket design purposes in that it predicts an averaged mass flux exponent that is too high and an axial dependence that is too great. This is not surprising because the law was developed for a hybrid configuration wherein the fuel is a slab and most practical hybrid motor designs employ a cylindrical fuel configuration. Hence, the standard practice today is to invoke the form of Marxman's regression rate law, augmented by coefficients and exponents derived from subscale tests. Hence, the spatially and temporally averaged regression rate law is written as:

$$\hat{\dot{r}} = a\hat{\overline{G}}_{ox}{}^{n}\hat{x}^{m} \tag{2}$$

In equation 2, the coefficient a and exponents *n* and *m* are propellant dependent constants that that are determined experimentally. Note that the averaging process makes it possible to express the average regression in terms of the oxidizer mass flux G_{ox} (an easily measured quantity) instead of the total mass flux G. This expression assumes that the regression rate is pressure independent. (Note that the coefficient a is not unitless therefore care must be taken to use consistent units. For the data presented herein, the units of the mass flux G_{ox} are g/cm^2-sec and the regression rate $\dot{r}$ is in mm/sec.)

Regression rate data, used to determine the regression rate power law relationship, are typically obtained from sub-scale testing of a fuel-oxidizer combination in a ground-based facility. Spatially and temporally averaged regression rate, determined by measuring the fuel mass and port diameter change, are plotted against the oxidizer mass flux and a nonlinear regression algorithm is then employed to compute the regression rate law coefficient(s) and exponents. Multiple combustion tests of single-port grains are often required to construct an average regression rate curve over a range of average oxidizer mass fluxes. In some modern testing facilities, the instantaneous regression rate is measured using ultrasonic or x-ray techniques to measure the instantaneous regression rate thus reducing the number of tests required. Using the traditional approach, a minimum of two (or three if $m \neq 0$) tests are required to construct a regression rate curve but ten or more are desirable for reasonable accuracy.

A complication that arises from experimentally determined regression rate laws based on a series of tests is that often they contain effects of temporal and spatial averaging that can mask important local regression rate behavior. Furthermore, the oxidizer-to-fuel ratio is usually not held constant from test to test hence the data should be O/F ratio corrected. Reference 3 describes these effects and suitable regression rate data reduction techniques to obtain an accurate and unambiguous average regression rate law.

Even though techniques exist to measure regression rate, the tests are often costly and typically the data has a greater degree of scatter than is desirable. A minor change to propellant formulation often necessitates a new test series.

An emerging route to obtaining fuel regression rate is through the use of computational fluid dynamic codes coupled with modules that model the fuel pyrolysis and chemical reactions. Good agreement was obtained by Serin[4] between the measured and computed regression rate of HTPB burned with GOX using the commercially available CFD-ACE code. Even so, currently, several limitations preclude the use of CFD in lieu of combustion tests including turbulence modeling, and the complexities of finite rate chemical reactions and fuel pyrolysis.

In the current paper, Marxman's regression rate law is revisited and used as a starting point in an attempt to derive a regression rate model of higher fidelity. Grain configuration and port entrance effects are included in the model. Factors that influence the magnitude of the average mass flux exponent n are considered. Previously published regression rate data are then compared with the modified model.

II. Analysis

A. Dimensionless Parameters of Hybrid Combustion

Several non-dimensional numbers are of interest in the modeling of the diffusion flames and they are summarized in Table 1.

Table 1. Dimensionless parameters.

Non-dimensional Number	Definition	Physical Meaning	Typical Value	Interpretation
Prandtl	$\Pr = \frac{c_p \mu_e}{k_g}$	momentum diffusivity / thermal diffusivity	≈ 1	Approximately the ratio of the velocity boundary layer thickness to the thermal layer thickness.
Schmidt	$Sc = \frac{\mu_e}{\rho D_{12}}$	momentum diffusivity / mass diffusivity	≈ 1	
Lewis	$Le = \frac{Sc}{\Pr} = \frac{k}{\rho_e c_p D_{12}}$	thermal diffusivity / mass diffusivity	≈ 1	Note that in some references $Le = \frac{\Pr}{Sc}$
Stanton	$St = \frac{Nu}{\mathrm{Re}\,\Pr} = \frac{h}{\rho_e u_e c_p}$	heat transferred / fluid thermal capacity	$<<1$	Modified Nusselt number
Nusselt	$Nu = \frac{hL}{k}$	total heat transfer / conductive heat transfer	$>>1$	Dimensionless temperature gradient at the surface.
Damkohler	$Da = \frac{t_t}{t_c}$	fluid dynamic time scale / chemical reaction time scale	$>>1$	$Da >> 1$ implies diffusion controlled combustion
Reynolds	$\mathrm{Re} = \frac{\rho_e u_e L}{\mu_e}$	inertial force / viscous force	$>>1$	

B. Fuel Regression Model

As mentioned previously, Marxman's regression rate law generally over predicts the fuel regression rate. An exception to this statement is for low regression rate fuels in a slab configuration. In this section, we will make use of computation and experimental evidence from several sources to support a few modifications to Marxman's theory in order to improve the regression rate prediction for cylindrical fuel grain configurations. The fuel-surface steady-state energy balance central to the model is shown schematically in figure 1.

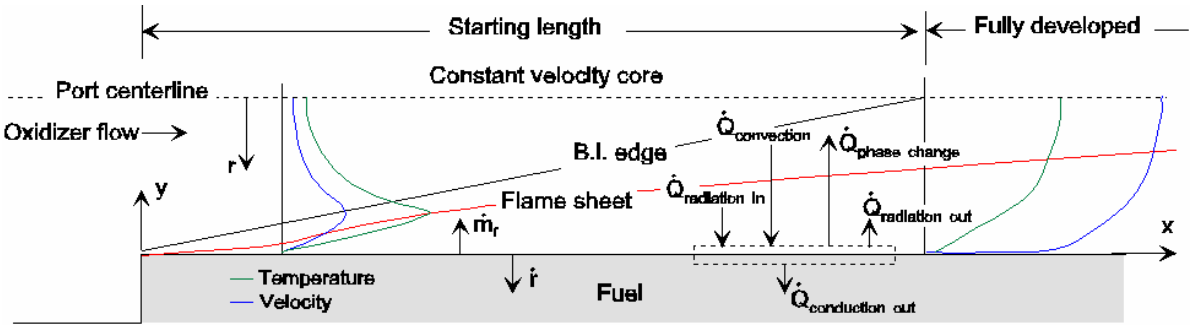

Fig. 1. Conceptualization of the flow and energy balance within hybrid rocket motor with a cylindrical port.

The essence of the model is that a thin flame sheet forms within a boundary layer on the fuel surface. The flame sheet is fed from below by vaporized fuel and from above by the port oxidizer flow. The fuel is vaporized primarily by convective heat transfer from the flame sheet to the fuel surface, although for some fuels (e.g. fuels containing metals) radiation can contribute to the vaporization process. The flame sheet forms at a location where the oxidizer to fuel mixture ratio is near but less than stoichiometric. It is assumed that the reaction rate is infinitely fast (i.e. Da>>1) and therefore the chemical kinetics of the reaction are not explicitly considered and the reaction rate is limited by diffusion of oxidizer and fuel into the flame sheet.

The flame-sheet approximation implies that the all chemical reactions are confined to an infinitely thin sheet. In reality, the flame sheet has been observed to be approximately 10% of the boundary layer thickness. Although the fuel port velocity profile is impacted by the fuel blowing, (i.e. transpiration from the fuel surface) changes to the velocity profile caused by the presence of the flame sheet are negligible[5]. It is a fairly safe assumption that the boundary layer flow in the port is turbulent from inception because of the transpiration of fuel from the surface. To simplify the analysis, boundary and thermal layer similarity is assumed resulting in fuel and oxidizer concentration profiles that are linearly dependent on the velocity profile.

At the fuel surface, the steady-state energy balance as shown in figure 1 is:

$$\dot{Q}_{convection} + \dot{Q}_{radiation\ in} = \dot{Q}_{conduction\ out} + \dot{Q}_{phase\ change} + \dot{Q}_{radiation\ out}$$

that can be written per unit surface area as:

$$k_g \left.\frac{\partial T}{\partial y}\right|_{y=0^+} + a e_g s T_f^{\,4} = k_f \left.\frac{\partial T}{\partial y}\right|_{y=0^-} + r_f \dot{r} h_g + e_s s T_s^{\,4} \tag{3}$$

Where h_g is the effective heat (enthalpy) of gasification. For many non-metalized fuels, radiation heat transfer can be neglected. At the fuel surface, the rate-of-heat transfer per unit area convected from the flame sheet to the surface is equal to that conducted , $\dot{Q}_s = k_g \left.\frac{\partial T}{\partial y}\right|_{y=0^+}$. Therefore the simplified fuel surface energy balance can be written as:

$$\dot{Q}_s = r_f \dot{r} h_g \tag{4}$$

Determining the heat transfer rate $\dot{Q}_s$ is the crux of the regression rate problem. In general, $\dot{Q}_s$ is dependent on many geometrical, combustion and flow related factors. An additional complication in a hybrid rocket motor is that the vaporized fuel leaving the fuel surface substantially decreases the rate of heat transferred to the surface and therefore the regression rate (aka the “blocking effect” caused by fuel blowing).

Since a direct measurement of $\dot{Q}_s$ is nearly impossible, one has to resort to similitude and analogies to estimate the heat transfer rate. Marxman employed the Reynolds analogy to estimate the heat transfer rate for a turbulent boundary layer in the absence of blowing. He then developed an expression for the reduction in heat transfer rate in a boundary layer with blowing. We will follow a similar course.

A Stanton number can be defined as $St_D = \dot{Q}_s \big/ r_b u_m \Delta h$ where Δh is the enthalpy difference between the flame sheet and the fuel surface. The energy equation can then be written in terms of the Stanton number as:

$$St_s \, r_b u_m \Delta h = r_f \dot{r} h_g \tag{5}$$

The goal now becomes to find a simple way to determine the Stanton number for the reacting flow environment within the fuel port.

In Marxman's original model, he assumed that $\Pr \approx 1$. This approximation allowed him to choose the Reynolds analogy, $St = c_f / 2$ over more complex correlations (e.g. Chilton-Colburn analogy, $St \Pr^{2/3} = c_f / 2$ that is valid for $0.6 < \Pr < 60$). Implicit in the $\Pr \approx 1$ assumption is that the thermal and velocity boundary layers are of the same thickness. Data[2,5] show that the flame sheet in a hybrid rocket motor resides within the boundary layer (as shown schematically in figure 1) at a y/d ranging from 0.1 to 1.0 (depending on the distance along the grain and the oxidizer choice) and therefore the thermal layer is thinner than the velocity layer and $\Pr > 1$. Furthermore, the Reynolds and Chilton-Colburn analogies break down for gas flows where there is a large temperature difference between the surface and the bulk flow resulting in properties that vary significantly. A relation recommended by Gambill[6] (eq. 6) that is applicable for heat flux levels of 1600 kW/m^2 or higher for a turbulent tube flow through a tube and is valid over a range of Prandtl numbers is the most appropriate analogy identified and so this is the correlation that we will use. Defining a Nusselt number as $Nu_D = \dfrac{h_x D}{k_b}$ where h_x is the local heat transfer coefficient and a Reynolds number $\mathrm{Re}_D = \dfrac{r_b u_m D}{m_b}$, then $St_D = \dfrac{Nu_D}{\mathrm{Re}_D \Pr}$ and:

$$St_D \Pr^{0.6} = \frac{0.021 \mathrm{Re}_D^{\,k}}{(T_s / T_b)^l} \tag{6}$$

In equation 6, St_D, $\Pr$ and Re_D are the local values (i.e. at x) with properties evaluated at the local bulk gas temperature T_b. The bulk temperature is an energy-averaged fluid temperature across a tube that will be approximated as the film temperature $T_b \approx (T_c + T_s)/2$. In reference 6, $k = -0.2$ and $l = 0.29 + 0.0019(x/D)$ but in the current context, k and l will remain a free parameters during the derivation. Fundamentally, equation 6 relates the convective heat transfer between a gas and a surface to the fluid friction for a flow through a tube. Equation 6, like all convective heat transfer correlations for turbulent flow, is empirical. It should be noted that if $T_s = T_b$, equation 6 is nearly equivalent to the Chilton-Colburn analogy for flow in a tube which in turn is nearly equivalent to the Reynolds analogy when $\Pr = 1$. The denominator of equation 6 compensates for variable gas properties caused by large temperature gradients.

In most hybrid rocket motors of practical interest, the grain configuration is cylindrical with length-to-port diameter ratios in the range of 5 to 50 and a fuel grain fore-end geometry that resembles a forward-facing

step. Therefore in the Reynolds number range of 10^4 to 10^6 (based on port diameter) typically encountered in hybrid rocket motors, it is expected that entrance effects should play a role. The HTPB-GOX cylindrical-port hybrid computational result shown in figures 2-4 illustrates this point. These results were obtained using an equilibrium-chemistry Navier-Stokes code on a channel configuration with a pre-combustion chamber. Clearly, the flow is not fully developed until $x/H = 41.2$ which is close to the port exit. Therefore, equation 6 must be modified to account for entrance effects.

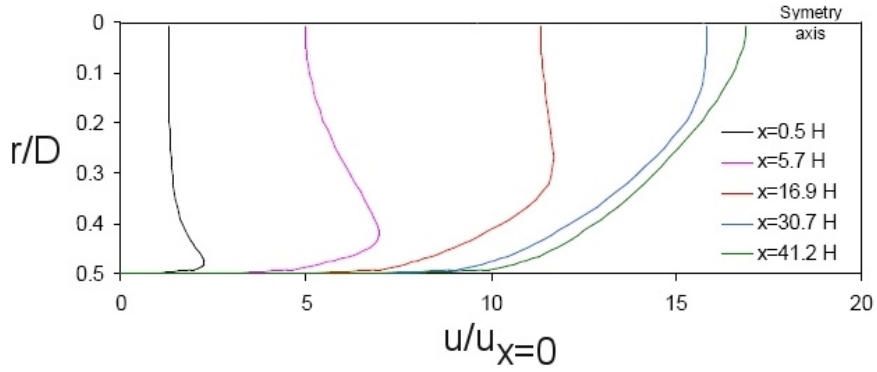

Fig. 2. Computed port velocity distribution, $u_{x=0} = 3.4$ m/sec (From reference 4).

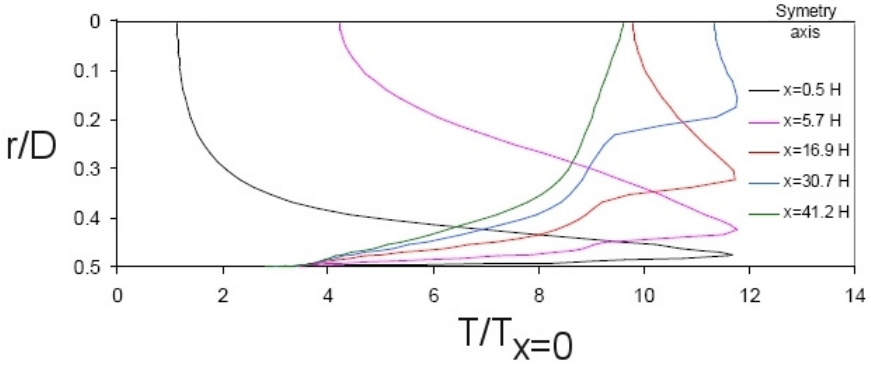

Fig. 3. Computed port temperature distribution, $T_{x=0} = 331$ K (From reference 4).

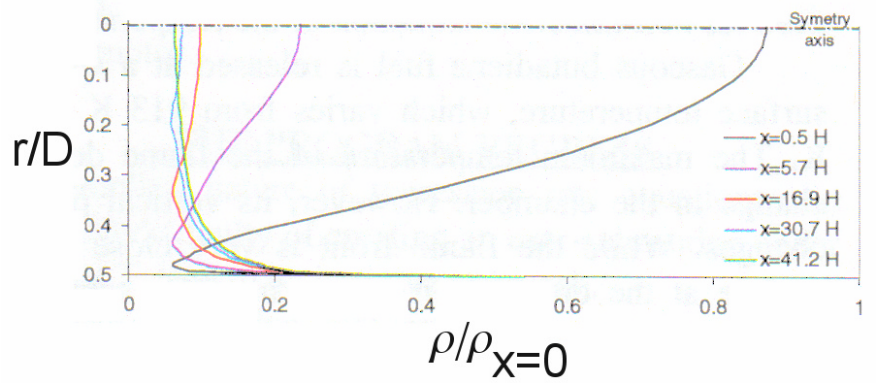

Fig. 4. Computed port density distribution $r_{x=0} = 43.3$ kg/m^3 (From reference 4).

In reference 7, experiments were performed to investigate the impact of a separated zone on the heat transfer in a pipe. These experiments are of interest because of their similarity to the flow at the inlet of a cylindrical fuel grain. In the experiments, a restriction was used within a heated pipe to create a separated zone. The effects of the restriction on the heat transfer were measured over a range of Nusselt, Reynolds and Prandtl numbers for a few restriction ratios. Presented in figure 5 is the ratio of local Stanton number St_x to the fully developed Stanton number St_D versus distance downstream of the restriction (note that the Stanton number ratio shown in figure 5 was calculated from Nusselt number data presented in reference 7). The data plotted is for a restriction diameter ratio of $d/D = 2/3$ which is considered to be representative of the entrance effects (i.e. right trends but magnitude is too high at $x/D \approx 2$) expected near the fore-end of a cylindrical fuel grain. As one can see in figure 5, a minor separation zone substantially increases the heat transfer for x/D less than about 10 over a range of Reynolds numbers. It should be noted that the boundary layer is turbulent and fully developed upstream of the restriction, and therefore the increased heat transfer is related to the restriction and not laminar or transitional flow.

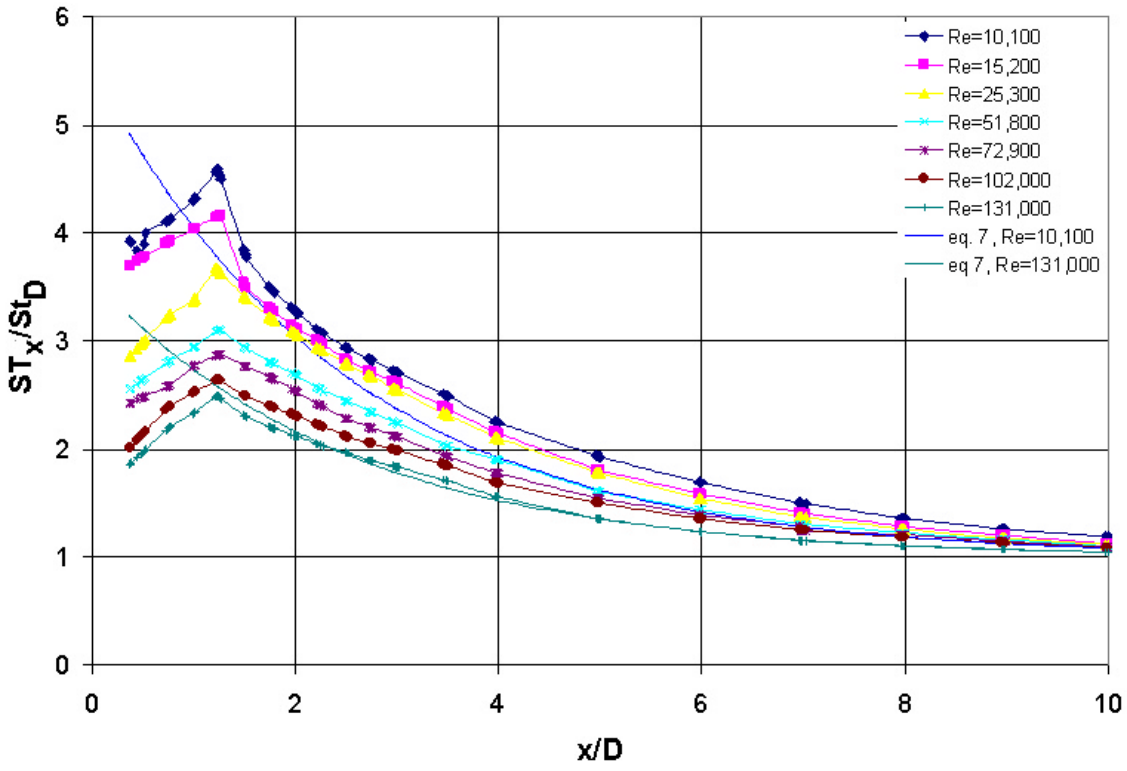

Fig. 5. Tube entrance effects on Stanton number (Pr=3, Nusselt number data source is reference 7).

It was difficult to find a simple function that would fit the data of figure 5 across the complete x/D range. Equation 7 was chosen because it is well behaved at large x/D and does a reasonable job for x/D greater than 1. For the comparison shown in figure 5, $C_1 = 34.6$ but based on data shown in other references and also the fact that the fuel port entrance becomes rounded during the burn, it is believed that $C_1 = 2.0$ will better represent the actual geometrically-induced entrance effects encountered in a fuel port and so this value will be used in the regression rate model.

$$\frac{St_x}{St_D} = 1 + C_1 \,\mathrm{Re}_D^{\,-0.22}\, e^{-0.4x/D} \tag{7}$$

In the paragraphs that follow, we will make use of several results that were derived for a zero pressure gradient turbulent boundary layer (e.g. flat plate boundary layer) with a thickness d and a characteristic velocity u_e at the boundary layer edge (subscript bl is used to distinguish boundary layer quantities from those expressed in terms of other characteristic velocities and length scales, e.g. a tube flow). In flows through cylinders without mass addition, the characteristic velocity typically employed is the mean velocity u_m which along with Re_D are assumed to be constant. In a hybrid fuel grain port, the velocity increases, the density decreases and the temperature increases with increasing x resulting in Re_D that is not constant with x. For instance, Re_D, based on port centerline quantities, decreases with x for the computational results presented in figures 2-4.

Marxman[1] defined a non-dimensional blowing coefficient $b_{bl} = \dfrac{(rv)_s}{r_e u_e c_f / 2}$ to quantify the mass addition to a boundary layer on a flat plate. He then derived a very fundamental result, namely, an expression for the velocity profile of a fully-developed turbulent boundary layer with mass injection. Boundary layer similarity is assumed and the result is valid for any boundary layer with a no-blowing velocity profile that follows a power law of the form $f_{bl} = \dfrac{u}{u_e} = h^n$ where $n << 1$. Typically, for a flat plate, $n = 1/7$ with $h = y/d$ and for a tube, $n = 1/9$ with $h = 2y/D$ when $b = 0$. The velocity profile with blowing that Marxman derived is: $f_{bl} = h^n \left(1 + \dfrac{b_{bl}}{2} h^n\right) \Big/ \left(1 + \dfrac{b_{bl}}{2}\right)$. The velocity ratio desired for flow through a cylinder is $f = \dfrac{u}{u_m} = f_{bl} \dfrac{u_e}{u_m}$. Using the definition of f_{bl} and $n = 1/9$, it can be shown that $u_e / u_m \approx 1.22$ for a tube-flow velocity profile with mass addition in the range of $5 < b < 100$ where u_e is the tube centerline velocity. For a tube, assuming the density does not vary significantly with y, the blowing coefficient can be defined as $b = \dfrac{(rv)_s}{r_b u_m c_f / 2}$, therefore $b = b_{bl} \dfrac{u_e}{u_m} = 1.22 b_{bl}$. Hence, for a tube:

$$f = \frac{1.22 h^{\frac{1}{9}} \left(1.22 + \dfrac{b}{2} h^{\frac{1}{9}}\right)}{1.22 + \dfrac{b}{2}} \tag{8}$$

As mentioned previously, fuel blowing reduces the heat transfer to the fuel. This effect can also be quantified in terms of a Stanton number ratio $\dfrac{St}{St_o}$ where St_o is the Stanton number without blowing. Marxman[2] invoked the Reynolds analogy coupled with the von Karman momentum integral equation to show that $\dfrac{St}{St_o} = \left[\dfrac{\ln(1 + b_{bl})}{b_{bl}}\right]^{4/5} \left[\dfrac{\dfrac{I}{I_o}}{1 + b_{bl}}\right]^{1/5}$ where $I = \dfrac{q}{d} = \displaystyle\int_0^1 \frac{ru}{r_e u_e} \left(1 - \frac{u}{u_e}\right) dh$ for a turbulent boundary layer with mass injection.[1,2,8] In performing the integration, a linear density variation was assumed between the surface and the edge of the boundary layer. He also showed that this result can be approximated by the simpler

expression $St/St_o \approx 1.2 b_{bl}^{-0.77}$ for $5 < b < 100$. He then used the Reynolds analogy to show that $b_{bl} = \frac{u_e}{u_c}\frac{\Delta h}{h_g}$. This is a very useful result because it quantifies the reduction of heat transfer to the fuel surface caused by blowing in a very succinct expression that is only a function of a velocity ratio and two thermodynamic properties. Chiaverini et al.[9] deduced a similar St/St_o correlation based on the results of HTPB-GOX motor tests (when slightly different blowing coefficient definitions are reconciled with each other). For a tube, $St/St_o \approx 1.4 b^{-0.77}$ and $b = 1.49\frac{u_m}{u_c}\frac{\Delta h}{h_g}$. The Marxman result will be used in the present analysis even though it was derived assuming that $\Pr = 1$. Since this term is a ratio of Stanton numbers, inclusion of the Prandtl number in the derivation would result in a quantity $\Pr/\Pr_o$ that should be close to one for most situations and therefore have a minimal impact on St/St_o.

So the Stanton number St_s in equation 5 should be replaced by the product $St_D\left(St_x/St_D\right)\left(St/St_o\right)$ where St_o is the Stanton number without blowing, St/St_o is the heat transfer decrement caused by blowing and St_x/St_D is the entrance effect. Combining equations 5 and 6 results in:

$$\dot{r} = \frac{0.021}{(T_s/T_m)^l}\Pr^{-0.6}\,\mathrm{Re}_D^{\,k}\left(St_x/St_D\right)\left(St/St_o\right)\frac{r_b}{r_f}u_m\frac{\Delta h}{h_g} \tag{9}$$

The local total mass flux is $G = r_b u_m$. Applying the variable definition $f_c = u_c/u_m$, substituting $St/St_o \approx 1.03\left(\frac{1}{f_c}\frac{\Delta h}{h_g}\right)^{-0.77}$ and equation 7 into equation 9 leads to the following local instantaneous regression rate expression:

$$\dot{r} = \frac{0.022}{r_f (T_s/T_m)^l}\Pr^{-0.6}\left[\frac{D}{m_m}\right]^k\left[1 + C_1\left(\frac{GD}{m_m}\right)^{-0.22} e^{-0.4x/D}\right]\left(\frac{\Delta h}{h_g}\right)^{0.23} f_c^{\,0.77} G^{k+1} \tag{10}$$

The above equation shows, among other things, that the position of the flame sheet relative to the fuel surface (as indicated f_c) has a first order impact of the heat transfer rate to the fuel and therefore the fuel regression rate. Marxman[2] used boundary layer integral methods along with species continuity equations to derive an expression for the velocity ratio for which the tube flow equivalent is

$f_c = \dfrac{1.22(O/F)\dfrac{\Delta h}{h_g}}{K_{ox_e} + (O/F + K_{ox_e})\dfrac{\Delta h}{h_g}}$ where O/F is the oxidizer to fuel ratio at the flame and K_{ox_e} is the oxidizer mass fraction at the edge of the boundary layer (usually unity). This relation is not immediately helpful because the local O/F is unknown but it does show the factors that influence flame stand-off distance including oxidizer choice.

In classic diffusion flame theory, the flame sheet resides at the location where the O/F is stoichiometric. In hybrid rocket motors, the diffusion flame is immersed in a turbulent boundary layer with mixing and transport aided by the eddy viscosity of the turbulent boundary layer. In addition, the flame sheet is observed to reside closer to the fuel surface (at a location where O/F is less than stoichiometric) in comparison to a classic diffusion flame. In Marxman's original modeling of PMMA burned with oxygen, the flame sheet was positioned at a fuel rich local O/F ratio of 1.5, (i.e. slightly less then the PMMA stoichiometric O/F of 1.92) without rigorous justification, (based on some measured results). In the current model, the flame sheet O/F ratio will be the stoichiometric value.

Equation 10 can be simplified by grouping variables that are approximately constant. It can be seen in figure 3 that the flame and surface temperatures are constant along the grain. Furthermore it can be assumed that the flame sheet resides at the same local flame O/F along the grain, therefore f_c is constant. These considerations make it possible to assume that $\Pr, m, \dfrac{T_s}{T_m}, \dfrac{\Delta h}{h_g}, f_c$ and r_f are independent of x and t and are roughly constant. Let:

$$A = \frac{0.022}{m_m{}^k (T_s/T_m)^l} \Pr^{-0.6} \left(\frac{\Delta h}{h_g}\right)^{0.23} f_c{}^{0.77} \tag{11}$$

Therefore the final form of the local instantaneous regression rate expression in terms of the total mass flux for a cylindrical grain is:

$$\dot{r} \approx \frac{A}{r_f}\left[1 + C_1\left(\frac{GD}{m_m}\right)^{-0.22} e^{-0.4x/D}\right] G^{k+1} D^k \tag{12}$$

Since the total mass flux G is a quantity that is difficult to measure, it is desirable to express the regression rate law in terms of the oxidizer mass flux G_{ox}. It takes several steps to accomplish this goal.

In equation 12, $G \approx G_{ox}$ in the term $C_1\left(\dfrac{GD}{m_m}\right)^{-0.22} e^{-0.4x/D}$ because at the fore end of the grain $G = G_{ox}$ and for increasing x, $e^{-0.4x/D} \to 0$. Therefore:

$$\dot{r} \approx \frac{A}{r_f}\left[1 + C_1\left(\frac{G_{ox}D}{m_m}\right)^{-0.22} e^{-0.4x/D}\right] G^{k+1} D^k \tag{13}$$

Conservation of mass written between the port entrance and x dictates that.

$$G(x) = G_{ox} + \frac{p\,D}{\frac{p\,D^2}{4}} \int_0^x r_f \dot{r} dx \tag{14}$$

Let's assume that fuel is added uniformly along the grain. We can then write the mass flux ratio G/G_o in terms of the $(O/F)_{x=L}$ at the end of the grain as:

$$\frac{G}{G_{ox}} = 1 + \frac{K_{ox}}{(O/F)_{x=L}} \frac{x}{L} \tag{15}$$

We can substitute equation 13 into equation 14 and then use equation 15 to get:

$$\frac{G}{G_{ox}} \approx 1 + \frac{4AG_{ox}{}^k}{D^{1-k}} \int_0^x \left[1 + C_1 \left(\frac{G_{ox} D}{m_m} \right)^{-0.22} e^{-0.4x/D} \right] \left(1 + \frac{K_{ox}}{(O/F)_{x=L}} \frac{x}{L} \right)^{k+1} dx \tag{16}$$

The integral in equation 16 can be integrated after using the binomial expansion $\left(1 + \frac{K_{ox}}{(O/F)_{x=L}} \frac{x}{L} \right)^{k+1} \approx 1 + \frac{(k+1)K_{ox}}{(O/F)_{x=L}} \frac{x}{L}$ and neglecting small terms (note that $k+1<1$ and $O/F_{x=l} > 1$). The result is:

$$\frac{G}{G_{ox}} \approx 1 + 4A(G_{ox}D)^k \frac{L}{D} \left[\frac{(k+1)}{2} \frac{K_{ox}}{(O/F)_{x=L}} \left(\frac{x}{L} \right)^2 + \left(\frac{x}{L} \right) - 2.5C_1 \left(\frac{D}{L} \right) \left(\frac{G_{ox} D}{m_m} \right)^{-0.22} \left(e^{-0.4x/D} - 1 \right) \right] \tag{17}$$

Comparing equation 15 and 17 and neglecting small terms, it can be seen that:

$$(O/F)_{x=L} \approx \frac{K_{ox}}{4A(G_{ox}D)^k} \frac{D}{L} \tag{18}$$

Equation 17 can be substituted into 13 to obtain the desired result of the local instantaneous regression rate in terms of the oxidizer mass flux G_{ox}:

$$\dot{r} \approx \frac{A}{r_f} \left[1 + C_1 \left(\frac{G_{ox} D}{m_m} \right)^{-0.22} e^{-0.4x/D} + 4A(k+1)(G_{ox}D)^k \frac{L}{D} \right] G_{ox}{}^{k+1} D^k \tag{19}$$

Where A is defined by equation 11.

Most measured regression rate results are temporally and spatially averaged results. Several approaches to averaging measured data are in common use and the techniques and the various pitfalls related to how the average oxidizer mass flux is defined are described in reference 3. As will be seen, it is difficult to obtain an exact closed-form solution for the modeled average regression rate and therefore similar techniques to that used for measured regression rate are invoked. A spatially and temporally averaged regression rate can be

defined as $\hat{\dot{\bar{r}}} = \frac{1}{t_b L}\int_0^{t_b}\int_0^{L} \dot{r}\, dx\, dt$. It is not possible to obtain an exact solution of this integral. The integration can be performed numerically, or for short burn times, it can be solved approximately. The approach taken here is to first perform the spatial average assuming a linear axial $\dot{r}$ variation. A spatially-averaged oxidizer mass flux can be written as $\overline{G}_{ox} = 4\dot{m}_{ox} / p\,\overline{D}^2$ where $\overline{D} = \left(D_{x=0} + D_{x=L}\right)/2$. The integral is:

$$\bar{\dot{r}} \approx \frac{1}{L}\int_0^{L} \frac{A}{r_f}\left[1 + C_1\left(\frac{\overline{G}_{ox}\overline{D}}{m_m}\right)^{-0.22} e^{-0.4x/\overline{D}} + 4A(k+1)\left(\overline{G}_{ox}\overline{D}\right)^k \frac{L}{\overline{D}}\right]\overline{G}_{ox}^{\,k+1}\overline{D}^{k}\, dx \tag{20}$$

Therefore, the spatially averaged regression rate is:

$$\bar{\dot{r}} \approx \frac{A}{r_f}\left[1 + 2.5C_1\left(\frac{\overline{G}_{ox}\overline{D}}{m_m}\right)^{-0.22} \frac{\overline{D}}{L} + 4A(k+1)\left(\overline{G}_{ox}\overline{D}\right)^k \frac{L}{\overline{D}}\right]\overline{G}_{ox}^{\,k+1}\overline{D}^{k} \tag{21}$$

A space-time averaged regression rate is given by $\hat{\dot{\bar{r}}} = \left(\overline{D}_f - \overline{D}_i\right)/2t_b$ and a space-time averaged port diameter can be defined as $\hat{\overline{D}} = (\overline{D}_i + \overline{D}_f)/2$, therefore the spatially and temporally averaged regression rate is given by:

$$\hat{\dot{\bar{r}}} \approx \frac{A}{r_f}\left[1 + 2.5C_1\left(\frac{\hat{\overline{G}}_{ox}\hat{\overline{D}}}{m_m}\right)^{-0.22} \frac{\hat{\overline{D}}}{L} + 4A(k+1)\left(\hat{\overline{G}}_{ox}\hat{\overline{D}}\right)^k \frac{L}{\hat{\overline{D}}}\right]\hat{\overline{G}}_{ox}^{\,k+1}\hat{\overline{D}}^{k} \tag{22}$$

Where $\hat{\overline{G}}_{ox} = 16\dot{m}_{ox} / p\left(\overline{D}_i + \overline{D}_f\right)^2$ and A is defined by equation 11.

As previously mentioned, the $\left(T_s/T_m\right)^l$ term of equation 6 was included to compensate for variable properties that arise from the extreme temperature gradients normal to the surface. It has been recognized by many that better high heat-flux correlations result with the explicit inclusion of a temperature dependency when properties are evaluated at the bulk temperature. The property most greatly impacted is viscosity which is strongly dependent on temperature. Physically, when the surface is cooler than the freestream, the boundary layer velocity profile is fuller in comparison to the isothermal flow because the viscosity is higher than that calculated using the equivalent bulk temperature. For most fuel grains, L/D is of the order 20 and therefore we can neglect the small dependency on x/D in the original exponent $l = 0.29 + 0.0019(x/D)$. Furthermore, equation 6 was established without considerations of mass addition and variable species, both of which have a major impact on local properties. Nevertheless, $l = 0.29$ will be used in the current model, and all properties related to the correlation will be evaluated at the bulk temperature.

The k exponent in equation 10 can be traced back to the Re_D exponent of the heat transfer correlation implemented (i.e. equation 6). This exponent has been confirmed to be -0.2 by many heated-wall tube-flow experiments. Even so, it is a bit of a stretch to expect that the correlation will work perfectly for a fuel port containing a chemical reaction, a flame zone and mass addition from the walls. Typical values of k found experimentally from regression rate tests range between -0.50 and -0.25 for fuels without metal additives and for some fuels containing metals, k approaches 0. All else being equal, the difference between $k = -0.2$ and $k = -0.5$ can result in a factor of 10 in regression rate. Therefore the accuracy of this exponent is critical to the success of a regression rate theory.

Several factors appear to have an impact on k including fuel composition, oxidizer choice, radiation and grain configuration (i.e. slab or cylindrical). Yet as the theory stands, k is a constant regardless of these factors. In reference 23, it was found that the pyrolysis Arrhenius constant E_a / RT_e, where E_a is the activation energy, was strongly correlated with the oxidizer mass flux exponent as determined from numerical solutions of a chemically reacting laminar boundary layer. A correlation of this type is not surprising because fuel production is related to the chemical degradation of the solid polymer even though the rate of the combustion chemical reaction is controlled by the interplay of heat transfer to the surface and diffusion of fuel and oxidizer into the flame zone. In the current model, without much of a physical basis at this point, the following relationship will be used (note that the flux exponent $n = k + 1$):

$$k = -0.005\left(\frac{E_a}{R_u T_s} \right) - 0.08 \tag{23}$$

This expression was determined by looking at n, E_a and T_s trends in the measured data of different propellant combinations.

Several points can be made concerning equations 19 and 22. Most importantly is that regression rate decreases with scale. For instance, increasing the diameter by a factor of ten while maintaining constant G_{ox} and L/D results in a regression rate decrease of 50%. A similar but not as pronounced scale effect was obtained computationally in reference 11. It should be noted that radiation (not included in the present model) should offset the regression rate scale effect to some degree. A second point to observe about equations 19 and 22 is that when equation 23 is implemented, the oxidizer flux exponent is around 0.7. This level is in line with that obtained experimentally for several common propellant combinations (and is less than the classical exponent of 0.8 that Marxman obtained). A final point is that both the instantaneous and average regression rate laws depend on a priori knowledge of the O/F at the flame sheet, (or alternately, f_c). This is the only quantity in the model that is not readily obtainable. It is expected that at some point, a theory will be developed that predicts the local O/F (and therefore, f_c) at the flame sheet location for a diffusion flame in a boundary layer. Until this occurs empiricism must be relied on to specify this quantity.

It should be reiterated that the model developed within this paper is most applicable to fuels that do not form significant melt or char layers. A char layer acts like an insulating blanket on the fuel surface that alters the heat transfer rate to the fuel. It may be possible to include the effects of char via a Stanton number ratio based on char number similar to the approach used to account for the blowing effect. The melt layer that forms on the surface of some high regression rate fuels (i.e. n-alkanes such as paraffin) results in a fuel entrainment mechanism into the flame zone that alters the basic fuel surface energy balance of equation 3.

Additional factors (aside from radiation effects) known to impact regression rate that are not incorporated in the model include the effects of fuel surface roughness, combustion chamber pressure (for some fuels) and combustion efficiency. Furthermore, finite rate chemical kinetics, additional aspects of fuel pyrolysis, and flame sheet curvature may be important for some fuel systems.

The local bulk temperature T_b is required in order to specify m_e. It can be seen in figure 3 that the temperature is highly variable throughout the domain with the temperature along the symmetry axis varying between T_{ox} at the inlet and T_c. The bulk temperature is computed approximately as $T_b \approx (T_c + T_s)/2$ where T_c is the adiabatic flame temperature computed by an equilibrium chemistry code. An additional complication is that the gas is a mixture of several species. During the fuel pyrolysis process, the polymer breaks down into low molecular weight volatile fuel species near the fuel surface. For HTPB burned with oxygen, the most prevalent species found between the surface and the flame zone are C_4H_6, C_2H_4, CH_4 and

CO. Above the flame, the main species are O_2, CO_2 and H_2O. Therefore determining the viscosity of the port gas is difficult. The approach taken here is to use the approximate formula[22] (from the Kinetic Theory of Gasses):

$$m_e = \left(26.69 \sqrt{\frac{MT_b}{s^2}} \right) \times 10^{-7} \qquad \frac{\text{kg}}{\text{m sec}} \tag{24}$$

Where M is the molecular weight, and s is the hard-sphere diameter in Angstroms and T_b is specified in K. As a rough approximation, it is assumed that on average, $M = (M_{ox} + M_{x=L})/2$ and $s = 5.0$ Angstroms (an average value). Fortunately, the viscosity in A of the regression rate expressions is raised to approximately the power of 0.2, so a factor of two change in T_b results in only an 8% difference in m_m. For averaged regression rate calculations, T_b is that found at $x = L/2$.

The effective heat of gasification h_g is the difference between the enthalpy of the solid in the initial state at ambient temperature and pressure, T_o and P_o and the enthalpy of the volatile thermally decomposed products at T_s and P_c:

$$h_g = \int_{T_0}^{T_s} c_p dT + \Delta h_f + \Delta h_d + \Delta h_v \tag{25}$$

Where Δh_f is the enthalpy of fusion, Δh_d is the enthalpy associated with fuel thermal degradation and Δh_v is the enthalpy of vaporization of the decomposed products. The effective heat of gasification is h_g is a quantity that can be measured in a constant heat flux gasification device or a flaming calorimeter. These measurements should be done under conditions that match the fuel surface regression rate.

In the model, the quantity Δh is the enthalpy change of the gas between the flame and the fuel surface. This quantity is dependent on the local O/F in addition to temperature. This quantity can be calculated using:

$$\Delta h = h_c - h_s = c_{p_c}(T_c - T_o) - c_{p_s}(T_s - T_o) \tag{26}$$

C. Fuel Regression Rate Data

The average regression rate for various commonly used hybrid rocket fuels burned with oxygen is shown in Figure 7 and data related to the burning tests that the regression rate curves were derived from are shown in Table 2. The curves shown were obtained by applying a nonlinear regression to measured data from many sources in the open literature over the oxidizer mass flux range encompassing the tests. Only data from cylindrical combustion chamber configurations are shown and no additional corrections beyond those of the original source have been applied.

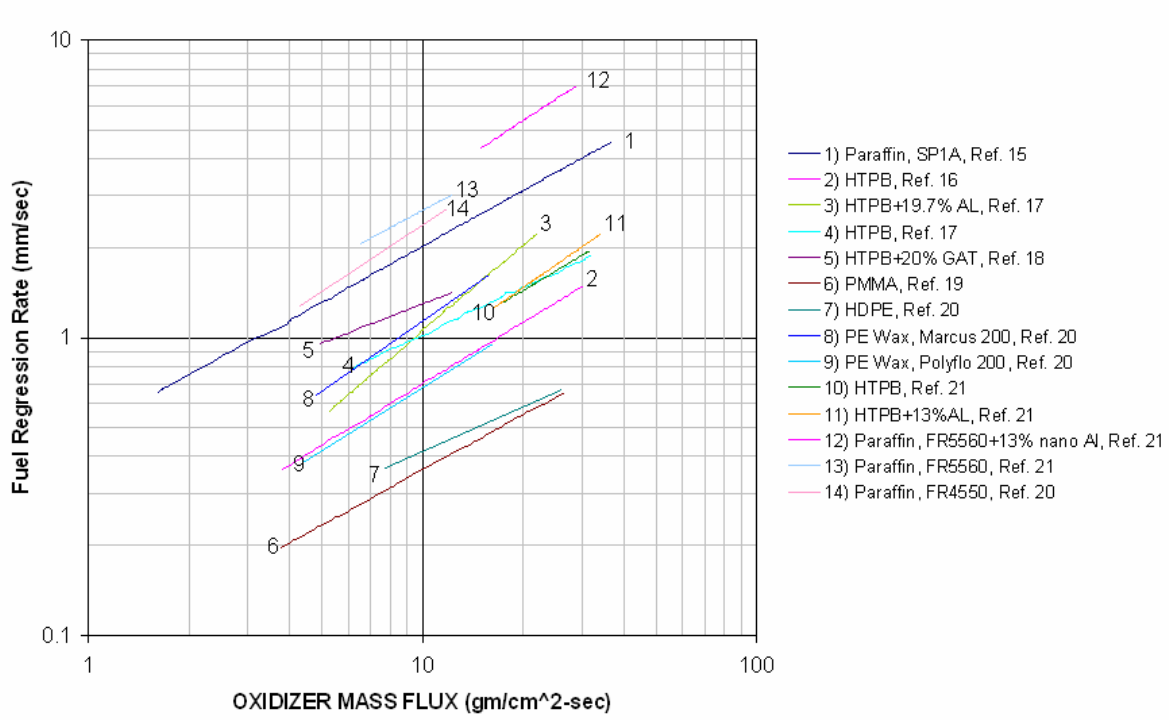

Fig. 7. Measured average fuel regression rate with oxygen.

Table 2. Data from regression rate tests.

Results summary of the average regression rate with oxygen for various fuels									
No.	Fuel	a †	n	No. of Tests	Chamber Pressure Range (MPa)	Average O/F Ratio Range	Data Reduction Technique	Oxidizer Mass Flux Range (g/cm^2-sec)	Ref.
1	Paraffin, SP1A	0.488	0.62	65	1.1-6.9	1.0-4.0	DA	1.6-36.9	15
2	HTPB, (Thiokol)	0.146	0.681	16	-	-	-	3.8-30.2	16
3	HTPB+19.7%AL	0.117	0.956	2	1.2	-	OA	5.1-23.0	17
4	HTPB	0.304	0.527	3	2.0	-	OA	6.2-31.0	17
5	HTPB+20%GAT	0.473	0.439	5	-	-	-	-	18
6	PMMA	0.087	0.615	8	0.3-2.6	-	-	3.3-26.6	19
7	HDPE	0.132	0.498	4	0.7-1.3	3.8-5.9	DA	7.7-26.1	20
8	PE Wax, Marcus 200	0.188	0.781	4	0.5-1.2	2.2-3.2	DA	4.8-15.8	20
9	PE Wax, Polyflo 200	0.134	0.703	3	0.6-1.2	1.6-1.7	DA	4.4-16.3	20
10	HTPB	0.194	0.670	6	-	-	OA	17.5-32.0	21
11	HTPB+13% nano Al	0.145	0.775	12	-	-	OA	16.5-34.2	21
12	Paraffin, FR5560 + 13% nano Al	0.602	0.730	8	-	-	OA	14.5-29.0	21
13	Paraffin, FR5560	0.672	0.600	4	-	-	OA	6.3-12.3	21
14	Paraffin, FR4550	0.427	0.748	3	0.7-?	1.3-1.8	DA	4.3-11.9	20

Regression rate equation: $\dot{\bar{r}} = a\overline{G_o}^{\,n} x^m$ with $m = 0$

† For use with G_o with units of gm/cm^2-sec, produces an average regression rate in mm/sec.
DA: Diameter Averaged, FA: Flux Averaged, AA: Area Average, OA: Other averaging technique applied

A couple of disclaimers are in order concerning the data presented in Fig. 7. Many factors including scale, O/F ratio, combustion chamber configuration, oxidizer injector design, fuel composition (i.e. trace additives) and processing, ignition and thrust termination transients, data reduction and experimental technique greatly impact the accuracy of reported regression rate data. This is one reason for the disparity between reported regression rate data for seemingly similar propellant combinations. An attempt was made to choose data from reliable sources, nevertheless, the data should be used for design purposes only and the actual regression rate of a fuel and oxidizer combination for any given application should be independently verified.

Fuel composition and processing can greatly affect the regression rate. This is particularly true for polymer-based fuels such as HTPB. Typical HTPB fuels are long-chain hydrocarbons that result from the mixing of a resin with a hardener and often a plasticizer, anti-oxidant, dispersant and an opacifier. The actual recipe and fuel processing techniques used varies widely and this information is usually closely held by companies as trade secrets.

D. Comparison of Model with Measured Data

The space-time average fuel regression rate predicted by the model developed in the preceding section is shown in figure 8 for three propellant combinations. The model was exercised using fuel grain dimensions equivalent to that of the test article. The Prandtl number in the model has been assumed to be equal to one uncertainty in the flame O/F ratio and port gas viscosity makes it difficult to determine a value of greater accuracy. Data supplied to the model is listed in Table 3 with the data source referenced where applicable. Several of the parameters used in the model were calculated using the thermo-chemistry code CEA that was developed at the NASA Glenn Research Center.

It was found that the model is very sensitive to specification of the fuel surface temperature T_s. Small adjustments in this temperature can easily result in a regression rate change of a factor of two. The surface temperature has an impact on the bulk temperature that is used in property determination and also on the k exponent, so it is understandable why this quantity is important. Since T_s is an input to the model and reliable measurements of T_s are difficult to obtain, (they must be performed under equivalent heat transfer rates in a specially designed test rig) some liberty was taken in the T_s value choice to produce a favorable regression rate match. The slope of the modeled results in figure 8 does not match the measured data very well. Since the slope is directly related to the oxidizer mass flux exponent n, the poor agreement is an indication that equation 23 could be improved. Finally, the port gas viscosity has a significant impact on the modeled results and this value has been determined using a very simple relationship (i.e. equation 24) that is probably not as accurate as desired.

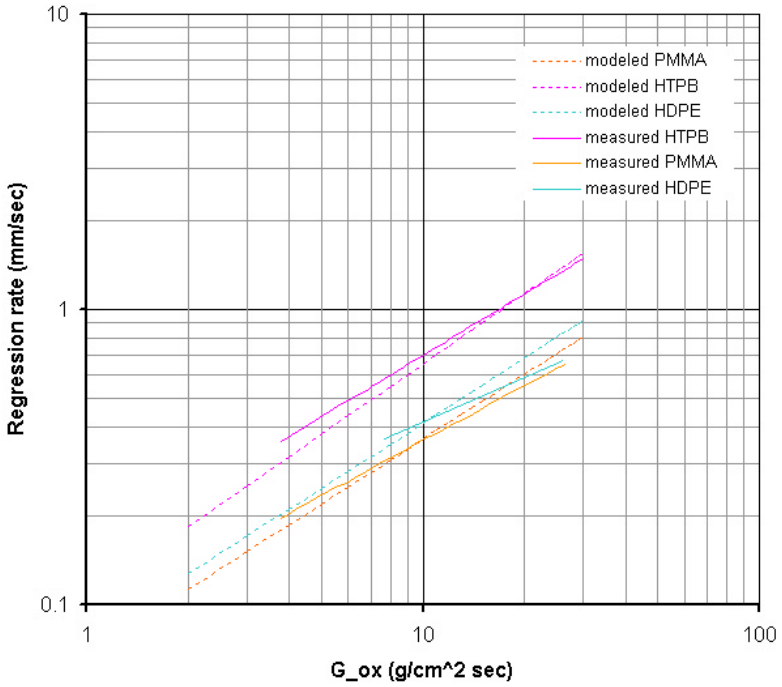

Fig. 8. Modeled average fuel regression rate with oxygen.

Table 3. Data used to determine the modeled fuel regression rate (with oxygen).

	PMMA	HDPE	HTPB
Average Formula	$(C_5H_8O_2)_n$	$(C_2H_4)_n$	$(C_{7.337}H_{10.982}O_{0.058})_n$
MW of repeat unit, (g/mol)	100	28	100
Δh_f, Heat of Formation (kcal/mole)	-102.9	-53.8 [13]	-2.97
O/F_{Stoic} †	1.92	3.0	2.7
O/F_{opt} (at optimal Isp_{vac}) †	1.7	2.7	2.5
T_c (at O/F, K) †	3483	3626	3701
T_s (K) *	500	840	935
M_{ex} (at O/F, g/mol) †	27.03	24.1	24.63
c_{p_s} (gas at surface, J/g K)	1.548 [11]	3.0	2.386 [11]
c_{p_c} (gas at flame, J/g K) †	7.16	8.02	7.88
Δh (eq. 26, J/g)	22306	24734	25296
h_g (J/g)	966 [11]	2200 [12]	1812 [11]
r_f (solid, kg/m^3)	1100 [11]	959 [12]	930 [11]

m_m (gas, eq. 24, kg/m sec) at T_m	1.29×10^{-4}	1.34×10^{-4}	1.37×10^{-4}
f_c (calculated using definition)	0.65	0.73	0.72
$E_a{}^*$ (kJ/mol)	160	264	203
$\overline{D}^{\wedge}$ (cm)	2.08	1.45	3.00
$L/\overline{D}^{\wedge}$	12.21	21.0	13.3
$^{\wedge}$ Values determined from grain configuration of test motor used in comparison			
† Calculated using CEA thermo-chemistry code, NASA Glenn.			
* from measured data under similar average regression rate conditions			

III. Conclusions

This paper presents a regression rate model that has been developed based on the results of several previous studies. The model is applicable to vaporizing fuels in a cylindrical grain configuration that do not form significant char or melt layers. It accounts for the presence of a pre-combustion chamber upstream of the fuel grain and also variable gas properties (to a limited degree). The model is compared with existing published regression rate data and the comparison is reasonable given the level of approximation in the model. The modeled oxidizer mass flux exponent is too high in comparison to that obtained by curve fits of measured data but it is closer to measured values than the exponent predicted by Marxman's classical regression rate theory.

The model is very sensitive to several parameters including the average fuel surface temperature and port gas absolute viscosity. The modeled regression rate can be off by a factor of two or more depending on the accuracy of the data used in the model. A major short coming of the model is the necessity of specifying the oxidizer-to-fuel ratio a priori (specified as stoichiometric even though the actual value may be less for some propellant combinations). Nevertheless, the model serves as a good starting point in assessing the factors that influence hybrid fuel regression rate.

Acknowledgment

This paper contains data and analysis originated under NASA cooperative agreements NAG3-2615 with the NASA Glenn Research Center and agreements NCC2-1172 and NCC2-1300 with the NASA Ames Research Center.

References

[1] Marxman, G. and Gilbert, M., "Turbulent Boundary Layer Combustion in the Hybrid Rocket," Ninth Symposium (International) on Combustion, Academic Press, 1963, pp 371-372.

[2] Marxman G. A., C. E. Wooldridge and R. J. Muzzy, "Fundamentals of Hybrid Boundary Layer Combustion", AIAA Heterogeneous Combustion Conference, Preprint No. 63-505, Palm Beach, Fl. Dec 11-13, 1963.

[3] Karabeyoglu, A., Cantwell, B.J. and Zilliac, G., "Development of Scalable Space-Time Averaged Regression Rate Expressions for Hybrid Rockets," AIAA/ASME/SAE/ASEE 41st Joint Propulsion Conference, Tucson AZ. AIAA 2005-3544, 2005.

[4] Serin, N and Gogus, Y.A., "Navier-Stokes Investigation on Reacting Flow Field of HTPB/O2 Hybrid Motor and Regression Rate Evaluation" AIAA 2003-4462, Huntsville, Al, 2003.

[5] Wooldridge, C. E. and Muzzy, R.J. "Measurements in a Turbulent Boundary Layer with Porous Wall Injection and Combustion." 10th Symposium (International) on Combustion, Academic Press, 1965, pp 1351-1362.

[6] Gebhart, B. *Heat Transfer*, 2nd Ed., McGraw Hill, New York, 1961.

[7] Krall, K.M. and Sparrow, E.M. "Turbulent Heat Transfer in the Separated, Reattached, and Redevelopment Regions of a Circular Tube," J. of Heat Transfer, Vol 88, No. 2, 1966. p. 131-136.

[8] Marxman, G.A., "Combustion in the Turbulent Boundary Layer on a Vaporizing Surface", 10th Symposium (International) on Combustion, Academic Press, 1965, pp 1337-1349.

[9] Chiaverini, M. J., Serin, N., Johnson, D., Lu, Y. C., Kuo, K. K., and Risha, G. A., "Regression Rate Behavior of Hybrid Rocket Solid Fuels ," *Journal of Propulsion and Power*, Vol. 16, No. 1, January-February 2000, pp. 125-132.

[10] Venkateswaran, S. and Merkle, C.L., "Size Scale-up in Hybrid Rocket Motors" AIAA-1996-647, Aerospace Sciences Meeting and Exhibit, 34th, Reno, NV, Jan. 15-18, 1996.

[11] Karabeyoglu, M.A., Altman, D. and Bershader, D., "Transient Combustion in Hybrid Rockets" AIAA 95-2691, 31st AIAA Joint Propulsion Conference, San Diego, CA 1995.

[12] Lyon, R.E. and Janssens, M.L., "Polymer Flammability," DOT/FAA/AR=05/14 May, 2005.

[13] Wilde, J.P. de , "The Heat of Gasification of PE and PMMA ", Memorandum M-593, Delft University of Technology, Delft, The Netherlands, 1988.

[14] Rabinovitch, B., "Regression Rates and Kinetics of Polymer Degradation," Tenth Symposium (International) on Combustion, Academic Press, 1965, pp 1395-1404.

[15] Karabeyoglu, A., Zilliac, G. Cantwell, B., De Zilwa S. and Paul Castelluci, " Scale-Up Tests of High Regression Rate Paraffin-Based Hybrid Rocket Fuels", Journal of Propulsion and Power, Vol 20., No. 6, Nov-Dec, 2004.

[16] Sutton, G.P. and Biblarz, O., Rocket Propulsion Elements, 7th ed. Wiley and Sons, New York, 2001.

[17] George, P. Krishnan, S., Varkey, P., Ravindran, M. and Ramachandran, L. "Fuel Regression Rate in Hydroxyl-Terminated-Polybutadiene/Gaseous-Oxygen Hybrid Rocket Motors," Journal of Propulsion and Power, Vol. 17, No. 1, 2001, pp 35-42.

[18] Hudson, M. K., Wright, A. M., Luchini, C., Wynne, P., and Rooke, S., "Guanidinium Azo Tetrazolate (GAT) as a High Performance Hybrid Rocket Fuel Additive", *J. Pyrotechnics*, No. 19, 2004, pp 37–42.

[19] Greiner, B., Federick, R, "Results of Labscale Hybrid Rocket Motor Investigation," AIAA/ASME/SAE/ASEE 28th Joint Propulsion Conference & Exhibit, Nashville, TN, AIAA, Paper 92-3301, 1992.

[20] Karabeyoglu, M, Cantwell, B. and Stevens, J. "Evaluation of Homologous Series of Normal-Alkanes as Hybrid Rocket Fuels," AIAA/ASME/SAE/ASEE 41th Joint Propulsion Conference & Exhibit, Tucson, AZ, AIAA, Paper 2005-3908, 2005.

[21] Evans, B. Favorito, A. and Kuo, K. "Study of Solid Fuel Burning-Rate Enhancement Behavior in an X-ray Translucent Hybrid Rocket Motor" AIAA/ASME/SAE/ASEE 41th Joint Propulsion Conference & Exhibit, Tucson, AZ, AIAA, Paper 2005-3909, 2005.

[22] Reid, R.C., Prausnitz, J.M. and Sherwood, T.K. *The Properties of Gases and Liquids,* 3rd ed., McGraw-Hill, New York, NY 1977.

[23] Krier, H., and Kerzner, H., "An Analysis of the Chemically Reacting Boundary Layer During Hybrid Combustion," AIAA 72-1144, AIAA Joint Propulsion Conference, New Orleans, LA, 1972.